

# Anomalous $WW\gamma$ coupling in photon-induced processes using forward detectors at the LHC

O. Kepka\*

*CEA/IRFU/Service de physique des particules, CEA/Saclay, 91191 Gif-sur-Yvette cedex, France  
IPNP, Faculty of Mathematics and Physics, Charles University, Prague and  
Center for Particle Physics, Institute of Physics, Academy of Science, Prague*

C. Royon†

*CEA/IRFU/Service de physique des particules, CEA/Saclay, 91191 Gif-sur-Yvette cedex, France*

We present a new method to test the Standard Model expectations at the LHC using photon-induced  $WW$  production. Both  $W$  decay in the main ATLAS or CMS detectors while scattered protons are measured in forward detectors. The sensitivity to anomalous  $WW\gamma$  triple gauge coupling can be improved by more than a factor 5 or 30 compared to the present LEP or Tevatron sensitivity respectively.

## I. INTRODUCTION

In this paper, we discuss a new possible test of the Standard Model (SM) predictions using photon induced processes at the LHC, and especially the  $WW$  production. The cross sections of these processes are computed with high precision using Quantum Electrodynamics (QED) calculations, and an experimental observation leading to differences with expectations would be a signal due to beyond standard model effects. The experimental signature of such processes is the decay products of the  $W$  in the main central detectors from the ATLAS and CMS experiments and the presence of two intact scattered protons in the final state.

It is foreseen to equip two LHC experiments, ATLAS and CMS, with very forward detectors which allow to detect intact scattered protons at very small angles after the collision. Together with the main central detector, they will help to identify inclusive and exclusive diffractive processes, two-photon exchange, etc. that would otherwise elude to be seen in the standard way with production in the central detector only. In this paper, we extend the physics diffractive program at the LHC by discussing  $WW$  production via photon induced processes. Two-photon interactions show a very clear experimental signature: two protons detected in the forward detectors and a certain number of well isolated leptons in the central (ATLAS or CMS) detector when at least one of the  $W$  decays leptonically. The activity in the central detector is devoid of any other particles since the interaction is due to the colorless exchange of two photons.

The theoretical success of the electroweak part of the SM lies in prescribing the underlying  $SU(2) \times U(1)$  symmetry to the fermion fields which not only implies the form of the coupling between fermions and gauge fields, but also leads to non-trivial predictions on interaction between the gauge fields themselves. It is quite difficult to measure the boson self-couplings because only the decay products of the bosons are observed and several different bosonic vertices can contribute to one observable process. The International Linear Collider is believed to be the machine for high precision measurement of the boson couplings but significant improvement of our knowledge of the boson self-interaction can be achieved already at the LHC.

The  $W$  pair production via two-photon exchanges shows a sufficiently high cross section to be observed at the LHC and a few thousand of such events can be observed in three years of LHC running at low luminosity. Using these data, one can directly measure the two-photon  $W$  pair production cross section and constrain the triple gauge coupling (TGC)  $WW\gamma$  and quartic gauge coupling (QGC)  $WW\gamma\gamma$  in  $pp \rightarrow pWWp$  processes through  $\gamma\gamma \rightarrow WW$ . Potential deviations from the SM expectation could indicate new physics beyond the SM. In this report we will show how the triple gauge boson vertex  $WW\gamma$  can be constrained using these topologies, by tagging the protons in forward detectors and observing the decay products of the  $W$  in the central detector.

The outline of this paper is as follows. We start by describing the forward detectors used in this measurement in Section 2. The concept of two-photon production will be overviewed in Sections 3 and 4 with the emphasis on the  $W$  pair production. In Section 5, we describe a measurement of the two-photon  $WW$  production cross section using forward detectors and discuss the background and resolution issues. Section 6 introduces the anomalous parameters for the  $WW\gamma$  vertex into the Lagrangian and derive the sensitivity on those couplings that could be achieved at the LHC using forward detectors.

---

\*Electronic address: kepkao@fzu.cz

†Electronic address: royon@hep.saclay.cea.fr

## II. FORWARD DETECTORS AT THE LHC

Following the experience from HERA [1] and the Tevatron [2] new detectors that can operate at the highest LHC luminosities are proposed to be installed in the LHC tunnel as an additional upgrade of the ATLAS and CMS detectors. These magnetic spectrometers measure precisely very forward protons and allow to study SM two-photon and diffractive physics such as  $W$  or jet production, search for the SM Higgs boson and also for new physics signals such as SUSY, in conjunction with the corresponding central detectors [3–5]. Protons which do not break up during collisions lose a small fraction of their momentum, are scattered at very small angles ( $< 100$  mrad) and continue to travel down the beam pipe. The bending magnets deflect them out of the beam envelope allowing the proton detection. Specifically for ATLAS and CMS, it is proposed to detect the protons at a distance of 220 m and 420 m from the ATLAS/CMS interaction point. Proton tracks can be reconstructed from hits in several layers of silicon 3D detectors that will approach the beam as close as 2 mm and 5 mm for 220 m and 420 m stations, respectively [6, 7].

A prime process of interest to be studied with forward detectors is the Central Exclusive Production (CEP)  $pp \rightarrow p + \phi + p$ , in which a single particle  $\phi$  such as Higgs boson or other (predominantly scalar) particle may be created in certain physics scenarios [3, 4, 8]. The observation of the new particle would allow a direct determination of its quantum numbers and a very precise determination of the mass, irrespective of the decay channel of the particle with a resolution between 2 GeV/c<sup>2</sup> and 3 GeV/c<sup>2</sup> per event [6, 7]. Exclusive production is a new phenomenon which was observed recently for the first time in the measurements of the CDF collaboration [9–13] and the confirmation and exploration of the CEP is a prime goal of the forward physics program, especially concerning the Higgs boson [14] and SUSY particle production [15].

## III. PHOTON-INDUCED PROCESSES AT THE LHC

Another important physics application of the forward detectors at the LHC are the photon-induced interactions. Processes in which at least one of the colliding particles emits almost real photons that subsequently enter the hard interaction have been already well explored at the electron-positron and proton-electron colliders at LEP and HERA, respectively. Very recently, photon-photon and photon-proton processes were also measured at a hadron-hadron collider by the CDF collaboration. In particular, CDF recorded isolated electron-positron pairs [16] with large rapidity gaps produced in  $pp \rightarrow p l^+ l^- p$  through  $\gamma\gamma \rightarrow l^+ l^-$  and also  $\Upsilon$  candidates in diffractive photoproduction  $pp \rightarrow p \Upsilon p$  through  $\gamma\mathbb{P} \rightarrow \Upsilon$  [17]. The obtained agreement between the two-photon dilepton production cross section measurement with the theoretical prediction proved that the definition of exclusive process at CDF was well understood and could in turn be applied for the exclusive two photon production [13].

As it was reviewed in [7], the LHC program of photon-induced interactions includes the two-photon production of lepton pairs that will be used for the independent luminosity measurement, two-photon production of  $W$  and  $Z$  pairs as a mean to investigate anomalous triple and quartic gauge couplings, two-photon production of supersymmetric pairs, associated  $WH$  photoproduction, and anomalous single top photoproduction. Last but not least, the dimuon two-photon production will be used for calibration and an independent alignment of the forward detectors at 420 m with respect to the beam on a store-by-store basis. During the low luminosity runs at the early stage of the LHC, it will be possible to identify two-photon processes without forward detectors. In this case one relies on the observation of the large rapidity gaps between the centrally created object and the forward protons. On the other hand, in order to run also at high instantaneous luminosity  $\mathcal{L} = 10^{33} - 10^{34} \text{ cm}^{-2}\text{s}^{-1}$  when up to 35 interaction per bunch crossing will occur, the operation of forward detectors is inevitable to distinguish whether the tagged proton come from the main  $\gamma\gamma$  interaction and not from a pileup event. In addition, the operation of forward detectors allows to reconstruct precisely the mass of the central object using the missing mass method as  $M = \sqrt{s\xi_1\xi_2}$  [18], where  $\xi_i$  is the momentum fraction loss of the protons  $\xi = (|\vec{p}| - |\vec{p}'|)/|\vec{p}|$ . The acceptance of the ATLAS forward detectors proposed by the ATLAS Forward Physics (AFP) Collaboration spans  $0.0015 < \xi < 0.15$  allowing the detection of object with masses  $100 \text{ GeV} < M < 800 \text{ GeV}$  with a good efficiency. The acceptance in CMS is similar.

## IV. TWO-PHOTON $W$ PAIR PRODUCTION

The two-photon production is described in the framework of Equivalent Photon Approximation (EPA) [19]. The almost real photons (low photon virtuality  $Q^2 = -q^2$ ) are emitted by the incoming protons producing an object  $X$ ,  $pp \rightarrow pXp$ , through two-photon exchange  $\gamma\gamma \rightarrow X$ , see Fig. 1. The photon spectrum of virtuality  $Q^2$  and energy  $E_\gamma$  then reads [19]

$$dN = \frac{\alpha}{\pi} \frac{dE_\gamma}{E_\gamma} \frac{dQ^2}{Q^2} \left[ \left(1 - \frac{E_\gamma}{E}\right) \left(1 - \frac{Q_{min}^2}{Q^2}\right) F_E + \frac{E_\gamma^2}{2E^2} F_M \right], \quad (1)$$

where  $E$  is the energy of the incoming proton of a mass  $m_p$ ,  $Q_{min}^2 \equiv m_p^2 E_\gamma / [E(E - E_\gamma)]$  the photon minimum virtuality allowed by kinematics and  $F_E$  and  $F_M$  are functions of the electric and magnetic form factors. They read in the dipole approximation [19]

$$F_M = G_M^2, \quad F_E = (4m_p^2 G_E^2 + Q^2 G_M^2) / (4m_p^2 + Q^2), \quad G_E^2 = G_M^2 / \mu_p^2 = (1 + Q^2 / Q_0^2)^{-4}. \quad (2)$$

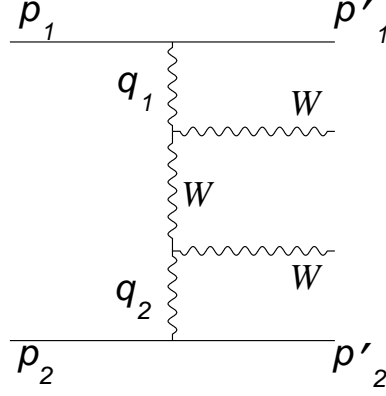


Figure 1: S-channel diagram, one of the three Feynman diagrams of the  $W$  pair production in two-photon processes. The others not shown correspond to a u-channel diagram and a diagram with direct coupling  $\gamma\gamma WW$ .  $p'_i$  are protons that do not break up but continue to travel down the beam pipe at small angles.

The magnetic moment of the proton is  $\mu_p^2 = 7.78$  and the scale  $Q_0^2 = 0.71 \text{ GeV}^2$ . The photon flux function falls rapidly as a function of the photon energy  $E_\gamma$  which implies that the two-photon production dominates the low mass region of the produced system  $W \approx 2\sqrt{E_{\gamma 1} E_{\gamma 2}}$ . After integrating the product of the photon fluxes from both protons over the photon virtualities and the energies while keeping the two-photon invariant mass fixed to  $W$ , one obtains the two-photon effective relative luminosity spectrum<sup>1</sup>. The effective  $\gamma\gamma$  luminosity at low  $W$  energy is shown in Fig. 2 in full line. The luminosity spectrum was calculated using the upper virtuality bound  $Q_{max}^2 = 4 \text{ GeV}^2$ . The luminosity spectrum after taking into account the forward detector acceptances  $0.0015 < \xi < 0.15$  is also shown in the figure in dashed line (it is calculated in the limit of low  $Q^2$ , thus setting  $E_\gamma = \xi E_{beam}$ ). Using the effective relative photon luminosity  $dL^{\gamma\gamma}/dW$ , the total cross section for a certain sub-process reads

$$\frac{d\sigma}{d\Omega} = \int \frac{d\sigma_{\gamma\gamma \rightarrow X}(W)}{d\Omega} \frac{dL^{\gamma\gamma}}{dW} dW, \quad (3)$$

in which the  $d\sigma_{\gamma\gamma \rightarrow X}/d\Omega$  denotes the differential cross section of the sub-process  $\gamma\gamma \rightarrow X$  that is a function of the invariant mass of the two-photon system. Finally, after multiplying the luminosity spectrum by the luminosity of the machine one obtains the two-photon production cross section.

The  $\gamma\gamma \rightarrow WW$  pair production is composed of three distinct Feynman diagrams (one of them is shown in Fig. 1). The complete formula of the differential cross section is listed in Appendix, see formula (9). Using formulae (3) and (9) and integrating over the two-photon mass  $W$  and spatial angles  $\Omega$ , one obtains the total cross section for  $W$  pair production through  $\gamma\gamma$  exchange in  $pp$  collision which is  $\sigma_{WW} = 95.6 \text{ fb}$ . This number was obtained for photons with an upper virtuality of  $Q_{max}^2 = 4 \text{ GeV}^2$  and photon energies  $0 < E_{\gamma 1,2} < 7 \text{ TeV}$ . No QED survival probability (to be discussed below) was taken into account.

Several extensions of the SM predict new physics at the TeV scale (e.g. low energy supersymmetry at about 1 TeV, new strong dynamics at about 1 TeV, low energy scale (quantum) gravity and extra large dimensions at a few TeVs). All models give a solution to the so called hierarchy problem, namely the question why the Plank mass  $M_{\text{Plank}} \simeq 10^{19} \text{ GeV}$  is huge compared to the electroweak scale  $M_{\text{EW}} \simeq M_Z$ . The observation and the measurements of photon induced processes with a photon invariant mass  $W > 1 \text{ TeV}$  is thus particularly interesting. The total production cross section of the  $W$  pairs with the invariant mass  $1 \text{ TeV} < W < 14 \text{ TeV}$  via two photon exchange is  $\sigma_{WW}(W > 1 \text{ TeV}) = 5.9 \text{ fb}$ . After taking into account the acceptance of the ATLAS or CMS forward detectors, the cross section falls to  $\sigma_{WW}(W > 1 \text{ TeV}) = 2.0 \text{ fb}$ . This means that it is expected to accumulate about 400  $WW$  events with an invariant mass above 1 TeV with a luminosity of  $\mathcal{L} = 200 \text{ fb}^{-1}$ .

## V. MEASURING THE $\gamma\gamma \rightarrow WW$ STANDARD MODEL CROSS SECTION

$\gamma\gamma \rightarrow WW$  is a very interesting process to measure precisely at the LHC since it incorporates the fundamental SM property of diagram cancellation. The SM model is a renormalizable theory. A necessary condition for the renormalizability of the theory

<sup>1</sup> We thank K. Piotrkowski for notifying us about the sign error in the photon spectrum formula published in [19]. For that reason we present the correct flux formula in Appendix (see Formula 8) for the reader's convenience.

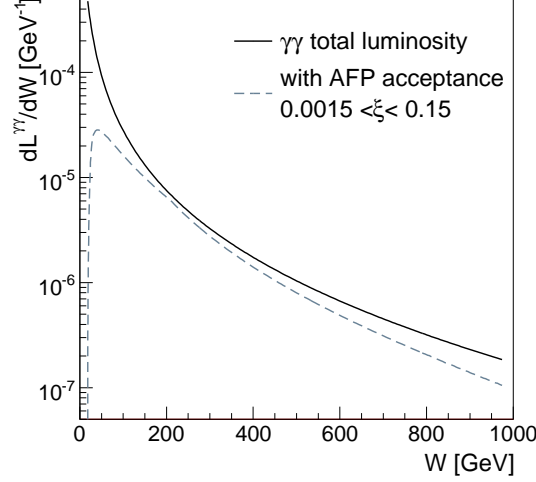


Figure 2: Relative effective  $\gamma\gamma$  luminosity in  $pp$  collisions at 14 TeV as a function of the two-photon invariant mass. The maximal virtualities of the emitted photons are set to  $Q_{max}^2 = 4 \text{ GeV}^2$ . The dashed curve shows the photon spectrum within the ATLAS or CMS forward detector acceptance.

into all orders is the so called “tree unitarity” that demands that unitarity is only minimally (logarithmically) violated in any fixed order of the perturbation series [20, 21]. More precisely the tree level unitarity means that any  $n$ -point tree level amplitude  $M_{tree}^n$  of the process  $1 + 2 \rightarrow 3 + 4 + \dots + n$  grows for the fixed nonzero angles in the high energy limit  $E \rightarrow \infty$  not faster than  $M_{tree}^n = O(E^{4-n})$ . In particular for the binary process of  $W$  pair production, the tree level unitarity implies that the scattering amplitude  $\gamma\gamma \rightarrow WW$  should turn constant in the high energy limit.

There are two diagrams with  $W$  exchange and one diagram with a direct  $\gamma\gamma WW$  coupling to be considered. The longitudinal polarization vector of the vector boson of nonzero mass grows linearly as a function of the boson momentum. Therefore each of the scattering diagrams alone is quadratically divergent in terms of the boson momentum in the high energy limit. However, the quadratic divergence is cancelled when all three diagrams are added and the total cross section is constant in the two-photon  $W_{\gamma\gamma}^2$  high invariant mass limit (the linear divergence arising in the case when only one of the vector bosons in the final state is longitudinally polarized is cured by introducing another scalar in the theory, the Higgs boson). It is thus very important to measure precisely the  $\gamma\gamma \rightarrow WW$  process since it incorporates the fundamental feature of the SM diagram cancellation.

The experimental signature of diboson events is very clear. Depending on the decay of the  $W$  there is zero, one, or two leptons in the final state. When both the  $W$  decay purely hadronically four jets are produced in the final state. This topology can be easily mimicked in the high luminosity environment with pileup interactions and also suffer from a high QCD background. Therefore this case is not considered in the following, and we always require that at least one of the  $W$  decays leptonically. In addition, the interpretation of the signal is simple contrary to e.g.  $e^+e^- \rightarrow WW$  production at LEP where such production could be due to  $\gamma$  or  $Z$  exchange and one could not clearly separate the  $WW\gamma$  and  $WWZ$  couplings. In our case, only the  $\gamma$  exchange is possible since there is no  $Z\gamma\gamma$  vertex in the SM.

In summary, we require the following constraints at particle level to select  $WW$  events:

- both protons are tagged in the forward detectors in the acceptance  $0.0015 < \xi < 0.15$
- at least one electron or muon is detected with  $p_T > 30 \text{ GeV}/c$  and  $|\eta| < 2.5$  in the main detector

The main source of background is the  $W$  pair production in Double Pomeron Exchange (DPE), i.e.  $pp \rightarrow p + WW + Y + p$  through  $\mathbb{P}\mathbb{P} \rightarrow WW + Y$  where  $Y$  denotes the pomeron remnant system. The rapidity gaps in DPE are smaller in size than in two-photon production because of the pomeron remnants and therefore it should be in principal possible to remove some part of the background by the rapidity gap size requirement. But running at high luminosity does not allow to rely on rapidity gap selection since gaps can be easily spoiled by particles coming from pile up interactions. The two-photon diboson production and the pomeron background were simulated using the Forward Physics Monte Carlo (FPMC) that was developed to enable event generation of all forward physics studies in one framework [22]. Besides the mentioned processes, it can simulate Central Exclusive Production in hadron-hadron collisions, single diffraction, diffraction at HERA, diffractive dissociation, etc.

The diffractive and two-photon production cross sections were multiplied by the survival probability factor, the probability that both the protons escape intact and are not destroyed by additional soft exchanges that might occur in addition to the hard interaction. Since the photon or pomeron included processes are of different nature, the corresponding survival probability differs. It is by more than one order of magnitude smaller (0.03) for the diffractive production than for the QED two-photon

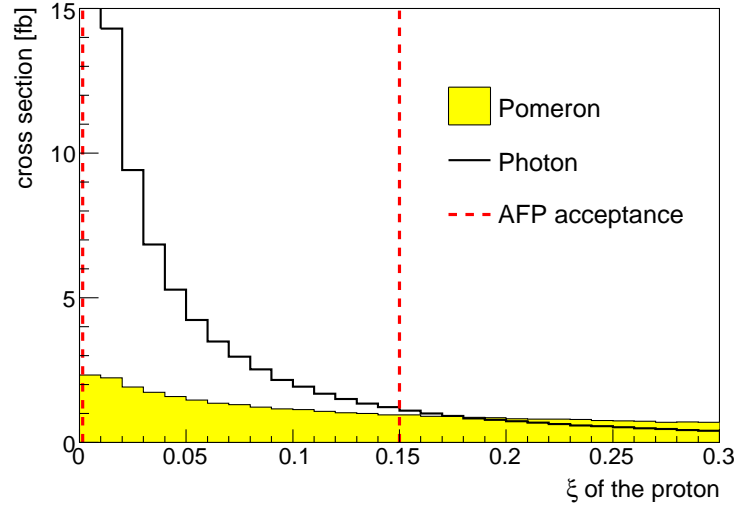


Figure 3:  $\xi$  dependence of the cross section for photon (black line) and pomeron induced events (shaded region). The former shows a steep  $\xi$  dependence while the pomeron background is suppressed by tagging the protons within the acceptance  $0.0015 < \xi < 0.15$ .

survival probability (0.8) [4]. Note that the survival probability for pomeron exchanges is model dependent (Ref. [23] and [24] predict respectively 0.01 and 0.03) and it will be one of the first diffractive measurements to be performed at the LHC. Hence the uncertainty due with the DPE background is about a factor of three, and we take the highest value predicted for the survival probability (0.03) to be conservative, which leads to the higher background DPE contamination. In summary, taking the survival probability factor into account, the total DPE  $WW$  production cross section is of the order of 67 fb.

To remove most of the DPE background, it is possible to cut on the  $\xi$  of the protons measured in the proton taggers. Indeed, two-photon events populate the low  $\xi$  phase space whereas DPE events show a flat  $\xi$  distribution, see Fig. 3. The lower proton momentum fraction  $\xi$  we can measure in the data sample within the forward detector acceptance, the higher signal (S) to background (B) ratio we obtain. A cut on the maximal value of  $\xi$  is applied in data to enhance the signal over background ratio. In table I, we give the signal and the background cross sections after analysis cuts requiring the presence of a reconstructed lepton (electron or muon) and the tag of both protons in forward detectors after different cuts on  $\xi$ . We also give the  $S/\sqrt{B}$  ratios for an integrated luminosities of  $200 \text{ pb}^{-1}$  and  $1 \text{ fb}^{-1}$ , respectively. The  $pp \rightarrow pWWp$  cross section can be measured precisely with a  $\mathcal{L}=1 \text{ fb}^{-1}$  with a statistical significance higher than  $20\sigma$  depending on the active  $\xi$  range. Using the full  $\xi$  acceptance  $0.0015 < \xi < 0.15$ , one expects about 30 tagged  $WW$  events. As the upper cut  $\xi_{max}$  decreases, one obtains a cleaner signal, but the number of observed events drops, see Tab. I. We note that already with a low integrated luminosity of  $\mathcal{L}=200 \text{ pb}^{-1}$  it is possible to observe 5.6  $W$  pair two-photon events for a background of DPE lower than 0.4, leading to a signal above  $8\sigma$  for  $WW$  production via photon induced processes.

$\xi_{max}$	signal [fb]	background [fb]	$S/\sqrt{B}$	$\mathcal{L}=200 \text{ pb}^{-1}$	$\mathcal{L}=1 \text{ fb}^{-1}$
0.05	13.8	0.16		15	34
0.10	24.0	1.0		11	24
0.15	28.3	2.2		8.6	19

Table I: Signal and background cross sections for  $\gamma\gamma \rightarrow WW$  production, and  $S/\sqrt{B}$  ratios for two luminosities ( $200 \text{ pb}^{-1}$  and  $1 \text{ fb}^{-1}$ ) as a function of the forward detector acceptance  $0.0015 < \xi < \xi_{max}$ . The presence of at least one reconstructed lepton is required as mentioned in the text.

## VI. ANOMALOUS $WW\gamma$ TRIPLE GAUGE COUPLING

New physics with a characteristic scale (i.e. the typical mass of new particles) well above what can be probed experimentally at the LHC can manifest itself as a modification of gauge boson couplings due to the exchange of new heavy particles. The conventional way to investigate the sensitivity to the potential new physics is to introduce an effective Lagrangian with additional higher dimensional terms parametrized with anomalous parameters. In this paper, we consider the modification of the

$WW\gamma$  triple gauge boson vertex with additional terms conserving  $C$ - and  $P$ - parity separately, that are parametrized with two anomalous parameters  $\Delta\kappa^\gamma$ ,  $\lambda^\gamma$  (a similar study discussing how to constrain the anomalous quartic coupling at the LHC using forward detectors can be found in [25]). The effective Lagrangian reads

$$\mathcal{L}/ig_{WW\gamma} = (W_{\mu\nu}^\dagger W^\mu A^\nu - W_{\mu\nu} W^{\dagger\mu} A^\nu) + (1 + \Delta\kappa^\gamma)W_\mu^\dagger W_\nu A^{\mu\nu} + \frac{\lambda^\gamma}{M_W^2}W_{\rho\mu}^\dagger W^\mu_\nu A^{\nu\rho}, \quad (4)$$

where  $g_{WW\gamma} = -e$  is the  $WW\gamma$  coupling in the SM and the double-indexed terms are  $V_{\mu\nu} \equiv \partial_\mu V_\nu - \partial_\nu V_\mu$ , for  $V^\mu = W^\mu, A^\mu$ . In the SM, the anomalous parameters are  $\Delta\kappa^\gamma = \lambda^\gamma = 0$ . The dependence of the total cross section on the anomalous parameters is shown in Fig. 4. The enhancement of the  $WW$  cross section is quite different for both couplings. It is strong for  $\lambda^\gamma$  where the cross section can be enhanced by more than two orders of magnitude. It is parabolic, monotonic for  $\Delta\kappa^\gamma$  in the interesting region around the SM values and the dependence on  $\Delta\kappa^\gamma$  is very weak. The event generation was carried out within the FPMC program [22] which was interfaced with the O'Mega matrix element generator [26] for this purpose. O'Mega constructs all possible LO contributions to particular process and generates a callable fortran function for the matrix element.

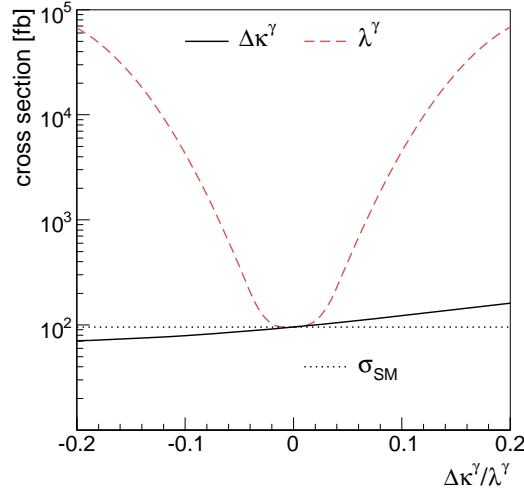


Figure 4: The full two-photon  $pp \rightarrow pWWp$  production cross section as a function of the  $WW\gamma$  anomalous coupling parameters  $\Delta\kappa^\gamma$  and  $\lambda^\gamma$  for  $\Lambda = \infty$ , i.e. with no form factor assumed. The SM value corresponding to  $\Delta\kappa^\gamma = \lambda^\gamma = 0$  is  $\sigma_{SM} = 95.6$  fb.

As was mentioned before, the SM couplings are defined in such a way that all tree level amplitudes fulfill the condition of tree level unitarity. This property is broken when additional terms of higher dimension are introduced in the Lagrangian. It is necessary to introduce a cut-off that removes the effect of the anomalous couplings in that limit in order to restore the tree level unitarity. Conventionally, this is done by introducing form factors in the dipole form

$$\begin{aligned} \Delta\kappa^\gamma &\rightarrow \frac{\Delta\kappa^\gamma}{(1 + s_{\gamma\gamma}/\Lambda^2)^n}, \\ \lambda^\gamma &\rightarrow \frac{\lambda^\gamma}{(1 + s_{\gamma\gamma}/\Lambda^2)^n}, \end{aligned} \quad (5)$$

where the  $\Lambda$  is a cut-off scale,  $n$  is an integer number and  $s_{\gamma\gamma}$  is the squared invariant mass of the photon-photon system. All the following calculations in which the form factors are taken into account were done setting  $n = 2$ . Most of analyses dealing with anomalous couplings use either no form factor  $\Lambda = \infty$  TeV or  $\Lambda = 2$  TeV. In order to compare our results with other approaches we will therefore systematically present our limits for both choices.

The anomalous parameters  $\Delta\kappa^\gamma$  and  $\lambda^\gamma$  have different effects on various observables. It turns out that the  $\Delta\kappa^\gamma$  changes mainly the normalization of the distributions whereas the  $\lambda^\gamma$  parameters modify the shape of the observables, which will be shown in the next section for some angular distributions. Here, the differential cross section is plotted as a function of the momentum fraction  $\xi$  in Fig. 5.  $\Delta\kappa^\gamma$  enhances the cross section any  $\xi$  in contrast to the  $\lambda^\gamma$  parameter which modifies the high  $\xi$  tail of the distribution. It is therefore desirable to perform a measurement at small  $\xi$  to get a good sensitivity to  $\Delta\kappa^\gamma$  but also to be sensitive to events at high  $\xi$  to observe the effect of the  $\lambda^\gamma$  anomalous parameter. Let us also note that it is useful to get an increased acceptance at high  $\xi$  to benefit from the large increase of the cross section when  $\lambda^\gamma$  is different from 0 since this enhancement appears only at high  $\xi$ . In the following, we will distinguish two cases: either we perform a “counting” experiment cutting only

on the  $\xi$  variable to enhance the effect of the anomalous coupling, or we use angular variables to allow to distinguish with the SM predictions.

The current best limits on anomalous couplings come from the combined fits of all LEP experiments [27].

$$-0.098 < \Delta\kappa^\gamma < 0.101 \quad -0.044 < \lambda^\gamma < 0.047. \quad (6)$$

The CDF collaboration presented the most stringent constraints on  $WW\gamma$  coupling measured at hadron colliders [28]

$$-0.51 < \Delta\kappa^\gamma < 0.51 \quad -0.12 < \lambda^\gamma < 0.13 \quad (7)$$

analyzing the  $W\gamma$  events in parton-parton interactions. Even though the LEP results are more precise than the results from the hadron collider, there is always a mixture of  $\gamma$  and  $Z$  exchange present in the process  $e^+e^- \rightarrow WW$  from which the couplings are extracted. The two-photon  $WW$  production have the advantage that pure  $W - \gamma$  couplings are tested and no  $Z$  exchange is present.

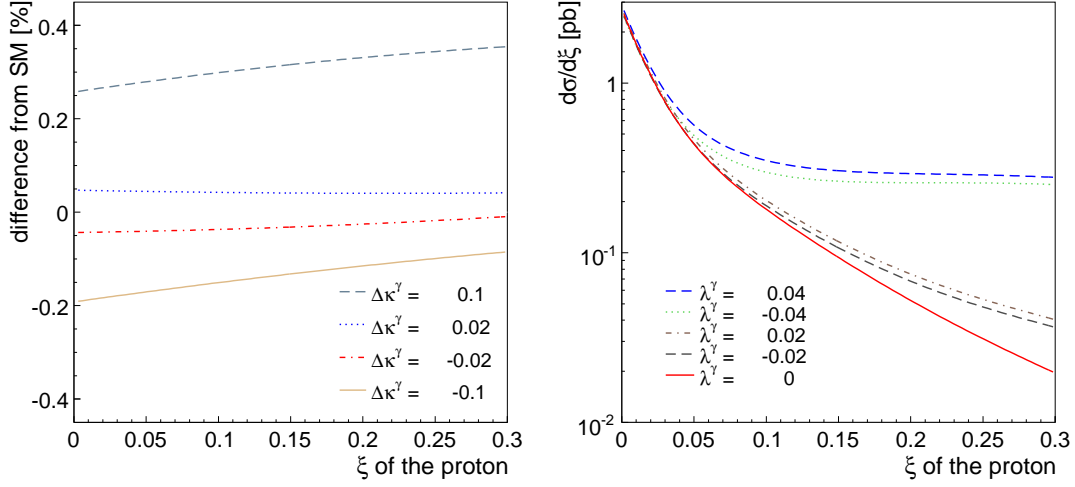


Figure 5:  $\xi$  dependence of the two-photon  $WW$  cross section for different values of  $\Delta\kappa^\gamma$  (left) and  $\lambda^\gamma$  (right) (SM values are 0). For  $\lambda^\gamma$ , the cross section is enhanced at high  $\xi$  which is at the edge of the forward detector acceptance ( $\xi = 0.15$ ). On the contrary, varying  $\Delta\kappa^\gamma$  in the interesting range ( $-0.05 < \Delta\kappa^\gamma < 0.05$ ) changes mainly the normalization and not the shape of the  $\xi$  distribution.

#### A. Sensitivity to anomalous parameters with the counting experiment

The sensitivity to anomalous coupling can be derived by counting the number of observed events and comparing it with the SM expectation. The statistical significance is defined as  $|\Delta N|/\sqrt{N_{SM} + N_P}$ , where  $\Delta N$  is the difference between the number of events predicted by the SM Lagrangian  $N_{SM}$  and the Lagrangian with nonzero anomalous parameters, and  $N_P$  denotes the number of events due to DPE background. This assumes that the background — pure diphoton SM and DPE — follows a Gaussian distribution. We consider two running scenarios with different acceptances of the forward detectors for AFP-CMS (AFP stands for ATLAS Forward Physics) and CMS-TOTEM experiments to derive the sensitivity on anomalous parameters:

- AFP-CMS - standard running condition of ATLAS or CMS/TOTEM forward detectors at 220 and 420 m with an acceptance of  $0.0015 < \xi < 0.15$ , which we mentioned already
- CMS-TOTEM - running with forward detectors around the CMS interaction point at 420 m and in addition the detectors of TOTEM experiment at 147 m and 220 m with an overall acceptance of  $0.0015 < \xi < 0.5$  (based on the Ref. [29]) as a mean to reach higher sensitivity<sup>2</sup> to  $\lambda^\gamma$ .

<sup>2</sup> Note that the study using the TOTEM acceptance up to  $\xi = 0.5$  should be seen as an approximate investigation of the physics potential since the precise determination of the TOTEM acceptance is still ongoing.

The TOTEM forward detectors are placed closer to the interaction point and hence have access to higher  $\xi$ . This is very desirable to enhance the sensitivity to  $\lambda^\gamma$  since the  $\lambda^\gamma$  signal manifests itself in the region of high  $\xi$  as we mentioned in the previous section (see Fig. 5).

In order to obtain the best  $S/\sqrt{B}$  ratio, the  $\xi_{min} < \xi_i < \xi_{max}$  acceptance was further optimized for the  $\lambda^\gamma$  parameter. The event is accepted if  $\xi_i > 0.05$  for the AFP-CMS scenario and if  $\xi_i > 0.1$  for the CMS-TOTEM scenario. These optimization cuts do not change significantly between studies with and without coupling form factors. In case of  $\Delta\kappa^\gamma$ , the full acceptance of the AFP detectors is used since the difference between the enhanced and SM cross section is almost flat around relevant values of the coupling  $|\Delta\kappa^\gamma| \sim 0.02$ , see Fig. 5 (left). To summarize, the corresponding acceptance cuts used to derive limits on the coupling parameters are shown in Table II.

	$\xi_{min}$	$\xi_{max}$
$\Delta\kappa^\gamma$ with AFP-CMS	0.0015	0.15
$\lambda^\gamma$ with AFP-CMS	0.05	0.15
$\lambda^\gamma$ with CMS-TOTEM	0.1	0.5

Table II: Different acceptances of the forward detectors used to derive the limits on TGCs for two running scenarios: AFP-CMS detectors and CMS-TOTEM forward detectors.

The dependence of the significance on the anomalous parameters multiplied by the form factors and calculated for an integrated luminosity of  $30 \text{ fb}^{-1}$  is shown in Fig. 6 for the AFP-CMS and CMS-TOTEM scenarios. The 95 % c.l. limits,  $3\sigma$  evidence and  $5\sigma$  discovery are indicated. The corresponding  $3\sigma$  evidence,  $5\sigma$  discovery and 95% confidence level limits derived for a luminosity of  $\mathcal{L}=30 \text{ fb}^{-1}$  are shown in Table III together with the limits obtained without form factors taken into account. As was mentioned above, the sensitivity to  $\lambda^\gamma$  is about two times better using the TOTEM roman pots at 147 m. The number of signal and background events is also given in Table IV for a 95% c.l. limit.

	form factor	$\Delta\kappa^\gamma(\text{AFP})$	$\lambda^\gamma(\text{AFP})$	$\lambda^\gamma(\text{CMS+TOTEM})$
95% c.l.	$\Lambda = \infty$	[-0.034, 0.029]	[-0.033, 0.026]	[-0.015, 0.014]
	$\Lambda = 2 \text{ TeV}$	[-0.051, 0.043]	[-0.041, 0.034]	[-0.018, 0.017]
$3\sigma$ evidence	$\Lambda = \infty$	[-0.053, 0.044]	[-0.038, 0.031]	[-0.017, 0.016]
	$\Lambda = 2 \text{ TeV}$	[-0.082, 0.064]	[-0.047, 0.040]	[-0.021, 0.020]
$5\sigma$ discovery	$\Lambda = \infty$	[-0.097, 0.069]	[-0.047, 0.038]	[-0.019, 0.018]
	$\Lambda = 2 \text{ TeV}$	[-0.154, 0.100]	[-0.055, 0.047]	[-0.024, 0.023]

Table III: 95% c.l.,  $3\sigma$  evidence, and  $5\sigma$  discovery potential on the  $WW\gamma$  anomalous parameters using AFP-CMS or CMS-TOTEM forward detectors with and without form factors applied for a luminosity of  $\mathcal{L}=30 \text{ fb}^{-1}$ .

form factor	$\Delta\kappa^\gamma(\text{AFP})$	$\lambda^\gamma(\text{AFP})$	$\lambda^\gamma(\text{CMS+TOTEM})$
$\Delta N$	60	15	25
$N_{SM}$	842	23	3
$N_{\text{P}}$	65	27	152
95% c.l.	[-0.051, 0.043]	[-0.041, 0.034]	[-0.018, 0.017]

Table IV: Number of signal events  $\Delta N$ , SM events  $N_{SM}$ , and background  $N_{\text{P}}$  to be observed for the values of anomalous couplings corresponding to the 95% c.l. limits for  $\Delta\kappa^\gamma$  and  $\lambda^\gamma$  (bottom line) in AFP-CMS and CMS-TOTEM running scenarios.

To study the best possible reach on measuring the anomalous parameters using the AFP-CMS detectors we derive the limits also for a luminosity of  $\mathcal{L}=200 \text{ fb}^{-1}$ . The significances were calculated in the same way as before and the results are summarized in Table V. We note that the present sensitivities coming from the Tevatron experiments can be improved by about a factor 30, while the LEP sensitivity can be improved by a factor 5.

A similar observation can be made using the distribution of the  $\gamma\gamma$  invariant mass. After tagging the protons with forward detectors, the invariant mass can be calculated as  $W_{\gamma\gamma} = \sqrt{s\xi_1\xi_2}$  with a resolution of 2-3 GeV. The signal due to the anomalous parameter  $\lambda^\gamma$  appears at high  $W_{\gamma\gamma}$  and induces a change in shape of the spectrum, see Fig. 7. At low  $W_{\gamma\gamma}$ , the dominant background to the anomalous signal is the SM two-photon production, whereas at high masses, the SM signal is very small and the background is mainly due to the DPE events. The situation is more favorable in case of CMS-TOTEM setup which has an acceptance to higher fractional momentum loss ( $\xi_{max} = 0.5$ ) and it is possible to tag higher  $\gamma\gamma$  mass, see Fig. 7 (right). The sensitivity on anomalous coupling is similar to the one we obtained using the counting experiment but cutting on  $W$ . The effect of the  $\Delta\kappa^\gamma$  anomalous coupling is to change the normalisation of the  $W$  distribution without modifying the shape. It means that the measurement of the  $W$  differential cross section is a way to distinguish between  $\lambda^\gamma$  and  $\Delta\kappa^\gamma$  couplings as well. It is



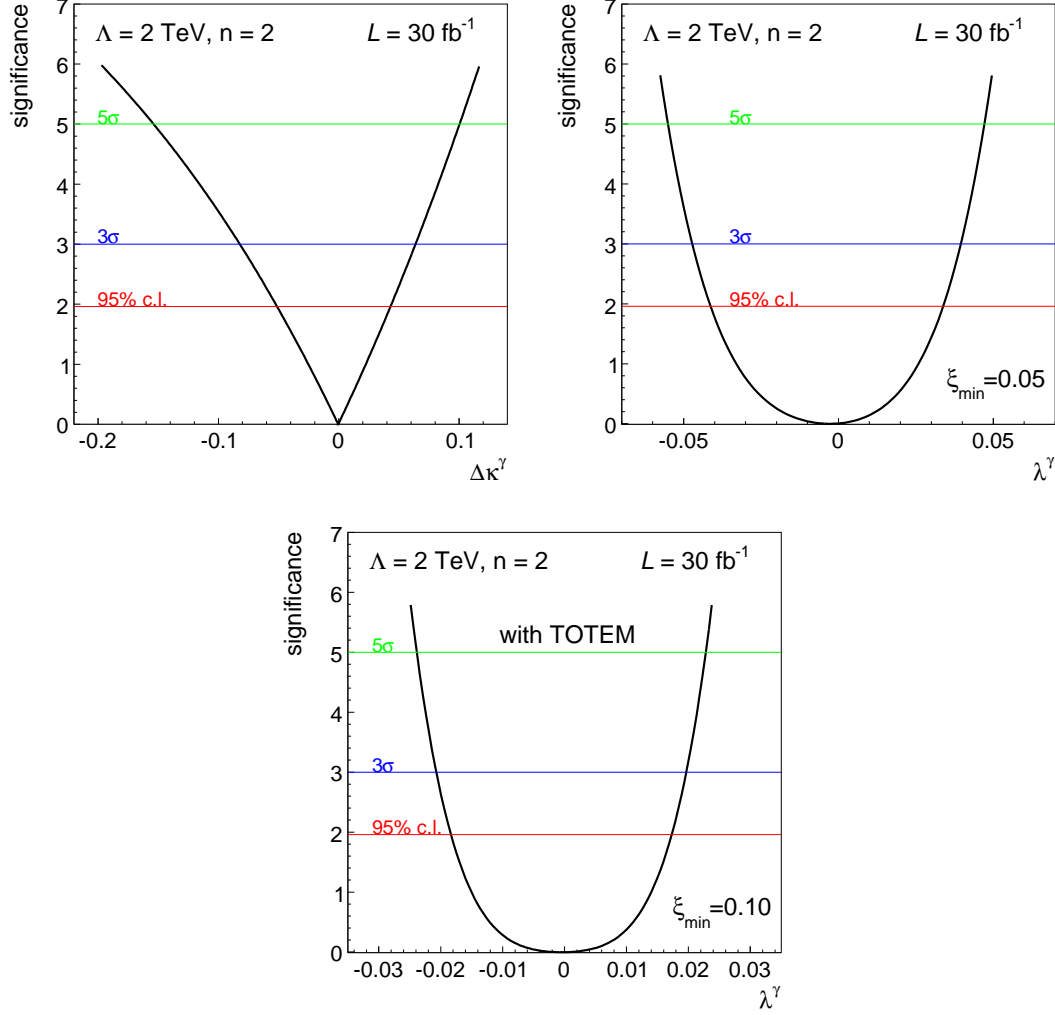


Figure 6: Significances as a function of the anomalous parameters  $\Delta\kappa^\gamma$  (left) and  $\lambda^\gamma$  (right) for  $\mathcal{L}=30 \text{ fb}^{-1}$  using the AFP-CMS forward detectors. The dependence on the anomalous parameter  $\lambda^\gamma$  using the CMS-TOTEM acceptance is also shown (bottom plot). The anomalous parameters were multiplied by the form factors (see equation (5)).  $\xi_{\min}$  is the minimum momentum fraction loss of the proton used to enhance the  $S/\sqrt{B}$  ratio.

also worth noticing that a binned likelihood fit of the  $d\sigma/dW$  shape of the distribution will allow to improve the sensitivity of  $\lambda^\gamma$  described in this paper once the forward detectors and their acceptance parameters will be well understood to distinguish between detector and physics effects.

### B. $p_T^l$ and angular distributions using an integrated luminosity of $\mathcal{L}=200 \text{ fb}^{-1}$

In this section we study some other observables related to angular distributions sensitive to anomalous parameters. However, it is needed to collect enough luminosity to be sensitive to a particular shape of the distributions and this is why we will study these distributions only for the highest luminosity,  $\mathcal{L}=200 \text{ fb}^{-1}$ .

Angular distributions computed at generator level are displayed in Fig. 8. The distribution of the angle between the leading lepton and the leading jet, the angle between the leading and the sub-leading lepton (ordered in  $p_T$ ), and the angle between the leading lepton and the vector of the missing energy in the event are shown. All shapes are significantly different when  $\lambda^\gamma$  is shifted from the SM value. We note that concerning the  $\Delta\kappa^\gamma$  parameter, the shape of the angular distributions is modified negligibly and cannot be used to derive better sensitivities by fitting the shape of the distributions.

The effect of the forward detector acceptance is such that the enhancement due to anomalous coupling is suppressed in the region where  $\lambda^\gamma$  enhances the cross section. For example, in Fig. 9 the angular distribution of the leading lepton- $E_T^{\text{miss}}$  angle

	form factors	$\Delta\kappa^\gamma(\text{AFP})$	$\lambda^\gamma(\text{AFP})$	$\lambda^\gamma(\text{CMS+TOTEM})$
95% c.l.	$\Lambda = \infty$	$[-0.013, 0.012]$	$[-0.024, 0.017]$	$[-0.011, 0.010]$
	$\Lambda = 2 \text{ TeV}$	$[-0.019, 0.017]$	$[-0.030, 0.023]$	$[-0.014, 0.013]$
$3\sigma$ evidence	$\Lambda = \infty$	$[-0.019, 0.018]$	$[-0.028, 0.021]$	$[-0.013, 0.012]$
	$\Lambda = 2 \text{ TeV}$	$[-0.029, 0.026]$	$[-0.035, 0.028]$	$[-0.016, 0.015]$
$5\sigma$ discovery	$\Lambda = \infty$	$[-0.033, 0.029]$	$[-0.033, 0.026]$	$[-0.015, 0.014]$
	$\Lambda = 2 \text{ TeV}$	$[-0.051, 0.042]$	$[-0.041, 0.034]$	$[-0.018, 0.017]$

Table V: 95% c.l.,  $3\sigma$  evidence, and  $5\sigma$  discovery potential on the  $WW\gamma$  anomalous parameters for a luminosity of  $\mathcal{L}=200 \text{ fb}^{-1}$  using the AFP-CMS or TOTEM-CMS detectors.

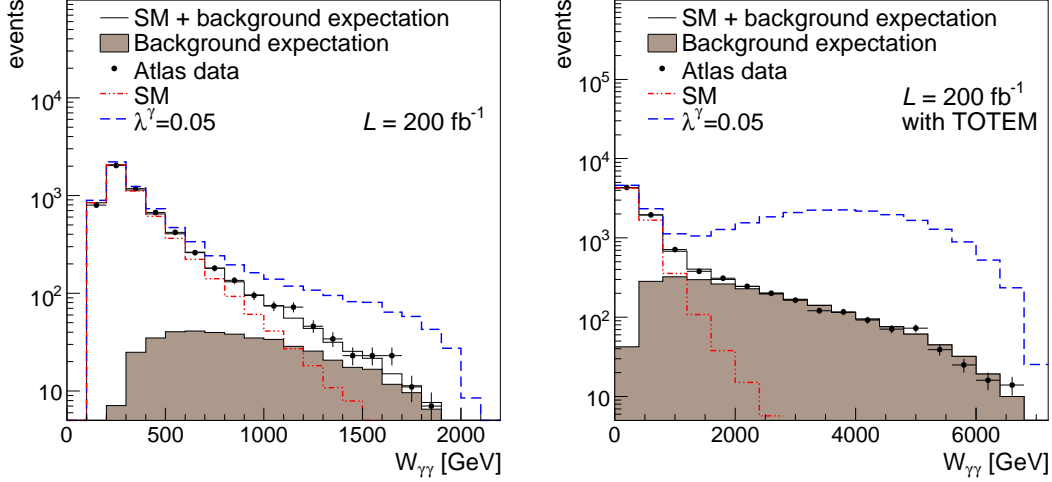


Figure 7: Distributions of the  $\gamma\gamma$  photon invariant mass  $W_{\gamma\gamma}$  measured with the forward detectors using  $W_{\gamma\gamma} = \sqrt{s\xi_1\xi_2}$  for AFP-CMS (left) and CMS-TOTEM (right). The effect of the  $\lambda^\gamma$  anomalous parameter appears at high  $\gamma\gamma$  invariant mass (dashed line). The SM background is indicated in dot-dashed line, the DPE background as a shaded area and their combination in full line. The black points show the ATLAS data smeared according to a Poisson distribution. The signal due to the anomalous coupling  $\lambda^\gamma$  is better visible when the full acceptance of TOTEM up to  $\xi = 0.5$  is used (right figure).

is shown for the DPE background, the SM and DPE background and the effect of anomalous coupling. Even though some enhancement is seen for a value of  $\lambda^\gamma = 0.05$ , it is much smaller than at generator level (Fig. 8). In addition, the distribution of the transverse momentum of the leading lepton is presented in Fig. 9. The signal due to the anomalous parameters appears in the region of high lepton transverse momentum.

Unfortunately, the forward detector acceptance does not allow to benefit fully from the shape difference between the SM model background and the signal, and this is why it is not easy to improve the sensitivities reached by the counting experiments described in the previous section. However, the DPE background is by one order of magnitude smaller than the two-photon  $W$  pair production and testing the shape of the observed distribution against the Monte Carlo prediction on the basis of the binned log-likelihood method could lead to some improvement on the  $\lambda^\gamma$  sensitivity.

### C. Comparison with other LHC measurements

In this section, we compare our results of the 95% c.l. limits with the standard methods used for instance in ATLAS [30] and [31], to determine if our new method to assess anomalous coupling is competitive at the LHC. Expectations for the CMS collaborations are found to be similar.

In the inelastic channel, the  $WW\gamma$  anomalous coupling is probed by fitting the  $p_T^\gamma$  of the photon distribution to the NLO expectations using the combined sample of  $W(e\nu)\gamma$  and  $W(\mu\nu)\gamma$  events or by fitting the transverse mass distribution  $M_T(WW)$  of the boson pair in events with two  $W$ s in the final state. The corresponding 95% c.l. limits obtained for  $\mathcal{L}=30 \text{ fb}^{-1}$  assuming  $\Lambda=2 \text{ TeV}$  and  $n = 2$  for the coupling form factors are shown in Table VI. The current analysis using the forward detectors in ATLAS has about the same precision as the analysis in the inelastic channel in ATLAS and is therefore complementary to that performed without tagging the forward protons (see Table III). In addition, the anomalous parameter  $\lambda^\gamma$  can be event better

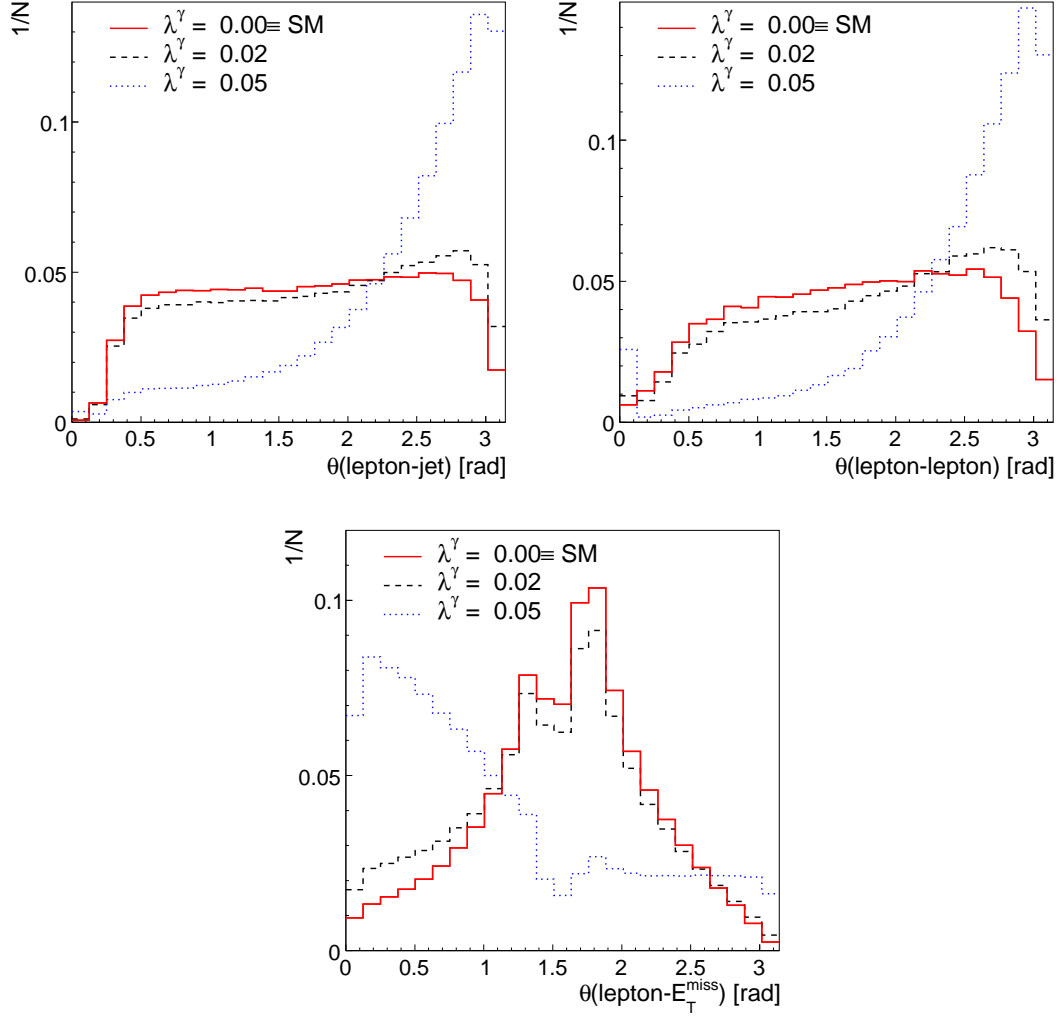


Figure 8: Various angular distributions for  $\lambda^\gamma = 0, 0.02, 0.05$ : angle between the leading lepton and the leading jet in the event (top left), angle between the two leading leptons in the event (top right), and angle between the leading lepton and the missing transverse energy at generator level. The shape of the angular distribution changes as a function of  $\lambda^\gamma$  (curves for negative values of  $\lambda^\gamma$  are not shown because they are similar to the ones with positive  $\lambda^\gamma$ ). Note that the shape of the angular distributions does not change with  $\Delta\kappa^\gamma$  and is therefore not shown here.

constrained if the  $\xi$  acceptance is larger as is in the CMS-TOTEM running scenarios mentioned above. In this case one gains about a factor 2-5 higher precision than in the conventional ATLAS analysis. Let us note also that the standard ATLAS analysis suffers from the difficult  $\gamma$  selection and energy scale whereas the presence of the forward detectors allows to perform an easier counting experiment.

	$\Delta\kappa^\gamma$	$\lambda^\gamma$
$W\gamma, (p_T^\gamma)$	[-0.11, 0.05]	[-0.02, 0.01]
$WW, (M_T)$	[-0.056, 0.054]	[-0.052, 0.100]

Table VI: 95% c.l. limits on the  $WW\gamma$  coupling parameters obtained from fitting the  $p_T^\gamma$  and  $M_T(WW)$  distributions in  $W\gamma$  and  $WW$  final states in inelastic production in ATLAS, and calculated for  $\mathcal{L}=30\text{ fb}^{-1}$  and for the form factors  $\Lambda = 2\text{ TeV}$ ,  $n = 2$ . [30].

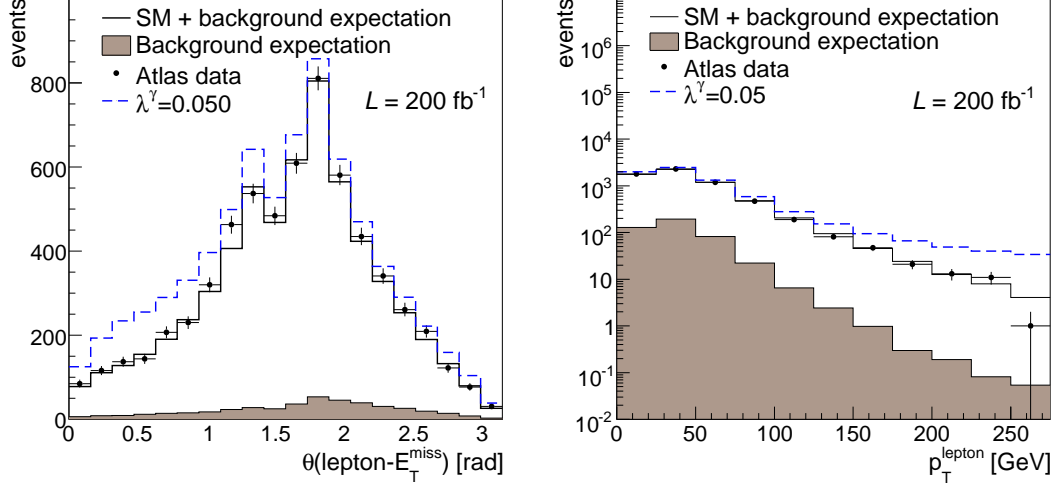


Figure 9: *Left*: distribution of the angle between the leading lepton and  $E_T^{miss}$ . *Right*: distribution of the leading lepton transverse momentum for  $\mathcal{L}=200\text{ fb}^{-1}$ . The DPE background is given in the shaded area (it is one order of magnitude smaller than the SM expectation), the SM and DPE background in full line and the effect of an anomalous coupling  $\lambda^\gamma = 0.05$  in dashed line. The black points show the ATLAS data smeared according to a Poisson distribution.

## VII. CONCLUSION

In this paper, we first discussed a new possible test of the SM by measuring the  $WW$  production via photon induced processes which has a cross section  $95.6\text{ fb}$ . This measurement assumes the detection of the decay product of the  $W$  in the main central detectors of ATLAS or CMS and the presence of forward detectors allowing to measure the intact scattered proton after the interaction. To remove most of the QCD background, only the cases when at least one of the  $W$  decays leptonically (electron or muon) is considered. After these assumptions, the cross section is of the order of  $28.3\text{ fb}$ , and most of the dominant background due to DPE can be removed by a cut on  $\xi < 0.15$ . With a low LHC luminosity of  $200\text{ pb}^{-1}$ , it is possible to observe a signal of  $5.6\text{ }WW$  events with a low background less than  $0.4$  events, leading to a signal above  $8.6\sigma$ . The measurement of the cross section can be compared to the precise QED expectation from the SM.

In a second part of the paper, we described how this measurement is sensitive to anomalous  $WW\gamma$  coupling. We considered the modification of the  $WW\gamma$  vertex with additional terms conserving  $C$  and  $P$  parity only, that are parametrized with two anomalous parameters  $\Delta\kappa^\gamma$  and  $\lambda^\gamma$ . The advantage with respect to LEP is that we are sensitive only to the  $WW\gamma$  coupling and not to the  $WWZ$  one. A simple counting experiment measuring the number of  $WW$  photon induced events and cutting on the  $\xi$  of the protons in the final state allows to gain about a factor 30 on anomalous couplings with respect to present sensitivity from the Tevatron, and a factor 5 compared to LEP results after accumulating  $200\text{ fb}^{-1}$ . Typically, the measurement extends to low  $\xi$  (down to  $0.0015$ ) and to high  $\xi$  (up to  $0.15$ - $0.5$ ) to obtain the best sensitivity to  $\Delta\kappa^\gamma$  and  $\lambda^\gamma$ , respectively. The best sensitivity on  $\Delta\kappa^\gamma$  and  $\lambda^\gamma$  is respectively  $[-0.013, 0.012]$  and  $[-0.011, 0.010]$ . Analyzing angular distributions at the LHC for instance between the leading lepton and the leading jet or the leading lepton and the sub-leading lepton only improves marginally the results since the region where most of the difference in shape appears is cut off by the forward detector acceptance.

Last but not least, it is worth mentioning that studying the differential  $WW$  production cross section via photon induced processes as a function of  $W$  is sensitive to beyond standard model effects (SUSY, new strong dynamics at the TeV scale, anomalous coupling, etc.) for  $W \sim 1\text{ TeV}$ . It is expected that the LHC experiments will collect 400 such events predicted by QED with  $W > 1\text{ TeV}$  for a luminosity of  $200\text{ fb}^{-1}$  which will allow to probe further the SM expectations. In the same way that we studied the  $WW\gamma$  coupling, it is also possible to study the  $ZZ\gamma$  one. The SM prediction for the  $ZZ\gamma$  coupling is 0, and any observation of this process is directly sensitive to anomalous coupling (the main SM production of exclusive  $ZZ$  event will be due to exclusive Higgs boson production decaying into two  $Z$  bosons).

## Acknowledgments

The authors thank K. Piotrkowski and M. Boonekamp for motivating this study and many discussions about it and in addition A. Kupčo, F. Chevallier, C. Marquet and R. Peschanski for reading the manuscript.

## Appendix

In this section we provide a list of formulae that were used for the calculation of the  $W$  pair production and are referenced in the text.

- The photon radiation by the proton is described by the photon spectrum. The photon spectrum in the Equivalent Photon Approximation is integrated from a kinematic minimum  $Q_{min}^2$  up to  $Q_{max}^2$  as a function of the photon energy  $E_\gamma$  and reads [19]

$$dN(E_\gamma) = \frac{\alpha}{\pi} \frac{dE_\gamma}{E_\gamma} \left(1 - \frac{E_\gamma}{E}\right) \left[ \varphi\left(\frac{Q_{max}^2}{Q_0^2}\right) - \varphi\left(\frac{Q_{min}^2}{Q_0^2}\right) \right], \quad (8)$$

$$\varphi(x) = (1 + ay) \left[ -\ln(1 + x^{-1}) + \sum_{k=1}^3 \frac{1}{k(1+x)^k} \right] \oplus \frac{(1-b)y}{4x(1+x)^3} + c(1 + \frac{y}{4}) \left[ \ln \frac{1+x-b}{1+x} + \sum_{k=1}^3 \frac{b^k}{k(1+x)^k} \right],$$

$$y = \frac{E_\gamma^2}{E(E - E_\gamma)}, \quad a = \frac{1}{4}(1 + \mu_p^2) + \frac{4m_p^2}{Q_0^2} \approx 7.16, \quad b = 1 - \frac{4m_p^2}{Q_0^2} \approx -3.96, \quad c = \frac{\mu_p^2 - 1}{b^4} \approx 0.028,$$

where  $\alpha$  denotes the Sommerfeld fine-structure constant,  $E$  the energy of the incoming proton, and  $Q_0^2 = 0.71$ .  $m_p$  is the proton mass and  $\mu_p \approx 7.78$  represents the magnetic moment of the proton. The circled plus sign in front of the second term corresponds to the fixed sign error of formula (D.7) in [19].

- The leading order differential formula for the  $\gamma\gamma \rightarrow WW$  process is a function of the Mandelstam variables  $s, t, u$  and the mass of the vector boson  $W$  [32]

$$\frac{d\sigma}{d\Omega} = \frac{3\alpha^2\beta}{2s} \left\{ 1 - \frac{2s(2s + 3M_W^2)}{3(M_W^2 - t)(M_W^2 - u)} + \frac{2s^2(s^2 + 3M_W^4)}{3(M_W^2 - t)^2(M_W^2 - u)^2} \right\}, \quad (9)$$

where  $\beta = \sqrt{1 - 4M_W^2/s}$  is the velocity of the  $W$  bosons.

- 
- [1] S. Alekhin *et al.*, arXiv:hep-ph/0601013.  
[2] K. Goulianos [CDF Collaboration], In *\*Hamburg 2007, Blois07, Forward physics and QCD\* 137-144*.  
[3] C. Royon, Mod. Phys. Lett. A **18**, 2169 (2003) and references therein;  
M. Boonekamp, R. Peschanski, C. Royon, Phys. Rev. Lett. **87** (2001) 251806; Nucl. Phys. **B669** (2003) 277;  
M. Boonekamp, A. De Roeck, R. Peschanski, C. Royon, Phys. Lett. **B550** (2002) 93;  
V.A. Khoze, A.D. Martin, M.G. Ryskin, Eur. Phys. J. **C19** (2001) 477; Eur. Phys. J. **C24** (2002) 581; arXiv:0802.0177;  
Phys. Lett. **B650** (2007) 41;  
A.B. Kaidalov, V.A. Khoze, A.D. Martin, M.G. Ryskin, Eur. Phys. J. **C33** (2004) 261; Eur. Phys. J. **C31** (2003) 387.  
[4] V. A. Khoze, A. D. Martin and M. G. Ryskin, Eur. Phys. J. C **23** (2002) 311.  
[5] N. Schul and K. Piotrkowski, arXiv:0806.1097 [hep-ph].  
[6] C. Royon [RP220 Collaboration], arXiv:0706.1796 [physics.ins-det].  
[7] M. G. Albrow *et al.* [FP420 R&D Collaboration], arXiv:0806.0302 [hep-ex].  
[8] M. Boonekamp, J. Cammin, R. Peschanski, C. Royon, Phys. Lett. **B654** (2007) 104.  
[9] O.Kepka, C. Royon, Phys. Rev.D**76** (2007) 034012.  
[10] M. Rangel, C. Royon, G. Alves, J. Barreto, R. Peschanski, Nucl. Phys. **B774** (2007) 53.  
[11] T. Aaltonen *et al.* [CDF Run II Collaboration], Phys. Rev. D **77** (2008) 052004.  
[12] Preliminary CDF result on Exclusive  $\chi_c$  Production <http://www-cdf.fnal.gov/physics/new/qcd/QCD.html>.  
[13] T. Aaltonen *et al.* [CDF Collaboration], Phys. Rev. Lett. **99** (2007) 242002.  
[14] S. Heinemeyer, V. A. Khoze, M. G. Ryskin, W. J. Stirling, M. Tasevsky and G. Weiglein, arXiv:0801.1974 [hep-ph].  
[15] M. Boonekamp, J. Cammin, S. Lavignac, R. B. Peschanski and C. Royon, Phys. Rev. D **73** (2006) 115011.  
[16] A. Abulencia *et al.* [CDF Collaboration], Phys. Rev. Lett. **98** (2007) 112001.  
[17] A. Abulencia *et al.* [CDF Collaboration], to appear.  
[18] M. G. Albrow and A. Rostovtsev, arXiv:hep-ph/0009336.

- [19] V. M. Budnev, I. F. Ginzburg, G. V. Meledin and V. G. Serbo, Phys. Rept. **15** (1974) 181.
- [20] J. M. Cornwall, D. N. Levin and G. Tiktopoulos, Phys. Rev. Lett. **30** (1973) 1268 [Erratum-ibid. **31** (1973) 572].
- [21] J. M. Cornwall, D. N. Levin and G. Tiktopoulos, Phys. Rev. D **10** (1974) 1145 [Erratum-ibid. D **11** (1975) 972].
- [22] M. Boonekamp, V. Juranek, O. Kepka, M. Rangel. C. Royon, to appear; see <http://cern.ch/project-fPMC/>
- [23] L. Frankfurt, C. E. Hyde-Wright, M. Strikman and C. Weiss, Phys. Rev. D **75** (2007) 054009.
- [24] E. Gotsman, E. Levin, U. Maor, E. Naftali and A. Prygarin, arXiv:hep-ph/0511060.
- [25] T. Pierzchala and K. Piotrkowski, arXiv:0807.1121 [hep-ph].
- [26] M. Moretti, T. Ohl and J. Reuter, arXiv:hep-ph/0102195.
- [27] J. Alcaraz *et al.* [ALEPH Collaboration], arXiv:hep-ex/0612034.
- [28] V. M. Abazov *et al.* [D0 Collaboration], arXiv:hep-ex/0803.0030.
- [29] V. Avati, K. Österberg, CERN-TOTEM-NOTE-2005-002, 2006.
- [30] ATLAS Standard Model Group Report, To be published.
- [31] M. Dobbs, M. Lefebvre, Atlas Note, Atl-Phys-2002-022.
- [32] A. Denner, S. Dittmaier and R. Schuster, arXiv:hep-ph/9601355.